J. Fluid Mech. (1982), *vol.* 116, *pp.* 431-458
Printed in Great Britain

An experimental study of the interaction between a glancing shock wave and a turbulent boundary layer

By HAYAO KUBOTA
Technical Research and Development Institute, Japan Defense Agency, Tokyo, Japan
AND JOHN L. STOLLERY
College of Aeronautics, Cranfield Institute of Technology, Bedford, England

(Received 7 April 1981)

The glancing interaction between an oblique shock wave and a turbulent boundary layer has been studied experimentally using a variable-incidence wedge mounted from the side wall of a supersonic wind tunnel. The Mach number was 2·3 and the Reynolds number 5×10^4, based on the 99·5 % thickness of the boundary layer just upstream of the interaction region. The study includes oil flow pictures, vapour and smoke-screen photographs, wall-pressure distributions and local heat-transfer measurements. The results suggest that the complicated interaction region involves two viscous layers: an induced layer formed from fluid initially in the boundary layer growing along the wedge surface near the root, and the thick turbulent layer on the tunnel side wall. The mutual interference between these layers is described, separation is defined and a discussion of incipient separation is included.

1. Introduction

On the surface of high-speed vehicles in transonic, supersonic or hypersonic flight, it is almost impossible to prevent some of the shock waves generated by the vehicle shape from interacting with the surface boundary layer. This interaction can cause a number of design problems, such as flow separation, loss of control or intense local heating. For two-dimensional flow the many theoretical and experimental investigations have had some success in describing the general flow features of the interaction. However, for the more practical case of three-dimensional interaction there are many unsolved problems. This is because of the large number of geometric variables, the general complexity of the flow structure and the experimental difficulties involved in resolving the physical phenomena.

Glancing interaction is one of the most important types of three-dimensional interference, in which an oblique shock wave crosses the path of a boundary layer growing along an adjacent wall. Our experiments used the simplest geometry, in which a variable-incidence wedge (shock generator) is mounted at right angles from a side wall (figure 1). This configuration is relevant to wing–fuselage, fin–tailplane and various intake-duct geometries.

The pressure rise across the oblique shock wave is 'smeared out' by the side-wall boundary layer so that the wall is covered by a disturbed flow pattern extending far upstream and downstream of the shock position in the free stream.†

† The position of the shock wave in the free stream, well away from the side wall, will be referred to here as the 'inviscid' shock position.

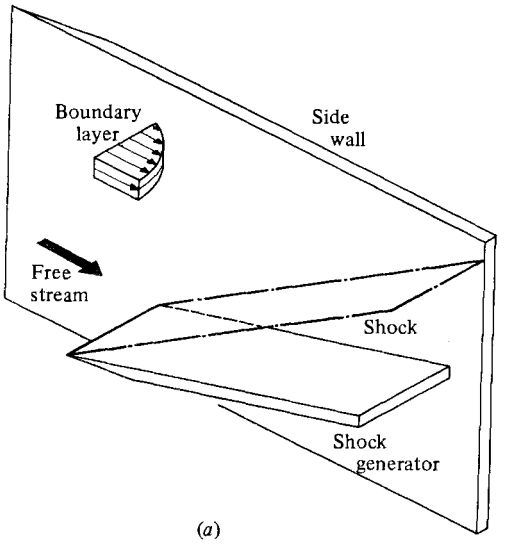

(*a*)

FIGURE 1 (*a*). Legend on facing page.

McCabe (1966) made one of the first important studies of glancing interaction, both theoretical and experimental. He noted that even for attached flow the pressure gradient on the side wall in the Y direction (see figure 1*b*) will deflect the sluggish boundary-layer fluid through a larger angle than the more vigorous external flow, as shown in diagram 1 of figure 2(*a*). Hence the boundary layer becomes highly skewed, and McCabe developed an approximate theory to calculate the surface-flow deflection angle assuming: (i) quasi-two-dimensional flow as shown in figure 2(*a*); (ii) that the vorticity in the boundary layer is convected downstream with the velocity of the local external flow. As an extension of this theory he tried to predict incipient separation (diagram 2 of figure 2*a*) by introducing a criterion based on his observations of the flow field. Accepting Maskell's (1955) definition of an ordinary separation line as an envelope of surface streamlines (figure 3*b*), McCabe suggested that incipient separation occurs when the deflected surface flow becomes aligned with the inviscid shock as shown in figure 2(*a*). By equating the theoretical surface-flow deflection angle to the inviscid-shock-wave angle, the wedge angle to induce incipient separation at any given free-stream Mach number could be calculated. For fully separated flow it was expected that the 'herringbone' type of surface flow pattern sketched in diagram 3 of figure 2(*a*) would be obtained.

Korkegi (1973) showed that at high Mach numbers McCabe's criterion could be approximated by the very simple relation

$$M_1 \delta_i = \left\{ \frac{4 - 3\sqrt{2}}{\gamma(\sqrt{2}-1) - (\sqrt{2}+1)} \right\}^{\frac{1}{2}}$$

where M_1 is the free-stream Mach number, δ_i is the shock generator angle (measured in radians) needed to induce incipient separation, and γ is the ratio of the specific heats. For $\gamma = 1{\cdot}4$ this relation becomes $M_1 \delta_i = 0{\cdot}364$, but Korkegi found that the best agreement with the experimental data was achieved using a value of 0·30. He went on to collect more data and showed that the simple formula

$$M_1 \delta_i = 0{\cdot}30$$

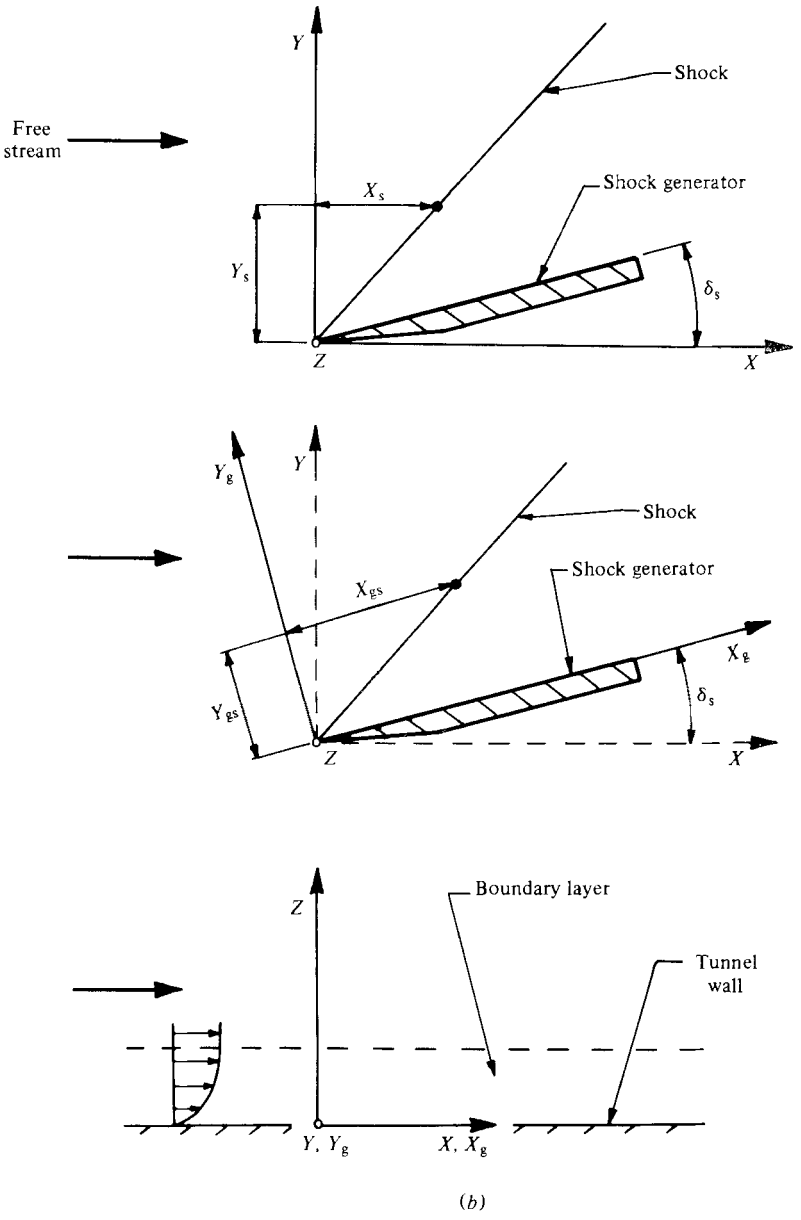

(*b*)

FIGURE 1. Glancing-shock boundary-layer interaction: (*a*) interaction region; (*b*) co-ordinate systems.

correlated the experimental results very well over the Mach number range $2 \leqslant M_1 \leqslant 6$ (Korkegi 1975). The correlation is shown in figure 4, but it is very important to recognize what is being portrayed. Strictly, figure 4 shows the wedge angle needed to turn the surface-flow lines through an angle equal to the inviscid-shock-wave angle. This wedge angle can be predicted reasonably well by $M_1 \delta_i = \text{const.}$† However, McCabe's suggestion for the incipient separation condition is not the only one.

† A further discussion of this point is made in §3.

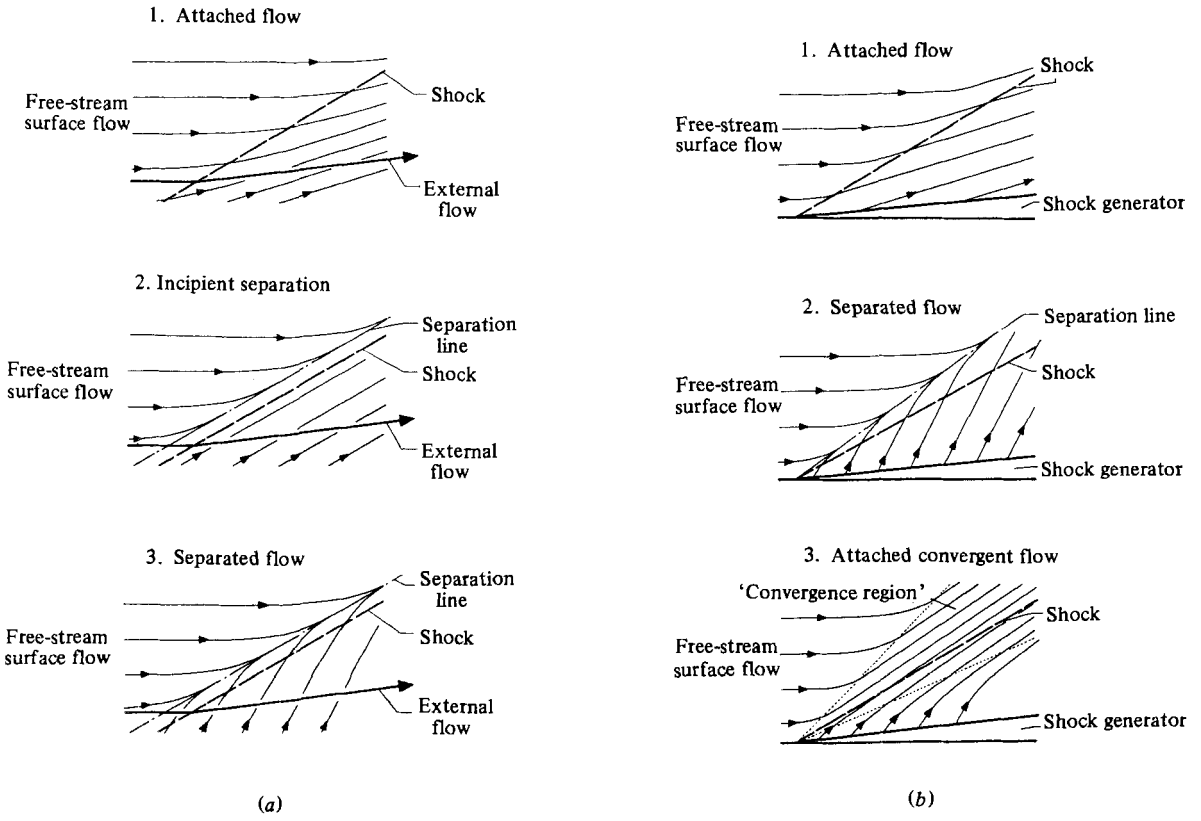

FIGURE 2. Surface-flow patterns in the interaction region: (*a*) quasi-two-dimensional flow field; (*b*) 'conical' flow field.

Oskam, Bogdonoff & Vas (1975) discussed in some detail the uncertainty in McCabe's criterion, mostly on the interpretation of their own oil-flow pictures and viscous-layer surveys. They concluded that, even when the surface-flow deflection exceeded the shock angle, the flow in the interaction region was attached. Although the oil streak lines were converging and tended to coalesce upstream of the shock, the lines did not converge into a single line. In fact the region of coalescence was growing in size along the direction of the swept shock, as shown in diagram 3 of figure 2(*b*), and labelled 'conical flow field – attached convergent flow'.

Other studies by Neumann & Token (1974), Neumann & Hays (1977), Token (1974) and Hays (1977) concentrated on the measurement of pressure and heat-transfer distributions, which are very important for practical applications. Attempts were made to correlate the peaks in pressure and local heating, and this work has been followed by the more recent paper by Scuderi (1978). Token (1974) sought to explain the high heat-transfer peak he measured on the side wall, near the root of the shock generator, by flow reattachment of a side-wall vortex. A sketch of his suggested 'vortex-dominated flow field' is shown in figure 5.

The present paper seeks to show the results from a wide variety of experimental techniques applied to a fairly large test-flow-field (23 × 23 cm) at a free-stream Mach number of 2·3. (Some of the results are compared with those from pilot experiments made in a 6 × 6 cm intermittent tunnel at $M = 2{\cdot}4$.) The measurements include

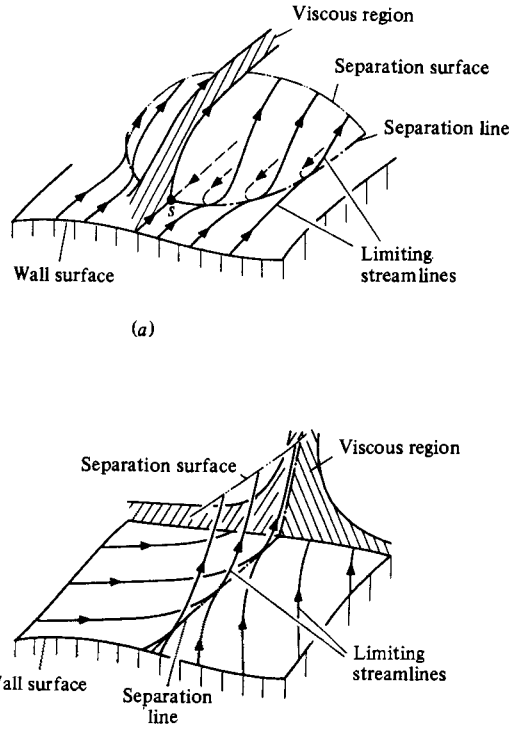

FIGURE 3. Separation models of Maskell (1955): (*a*) singular separation (*S* denotes singular point); (*b*) ordinary separation.

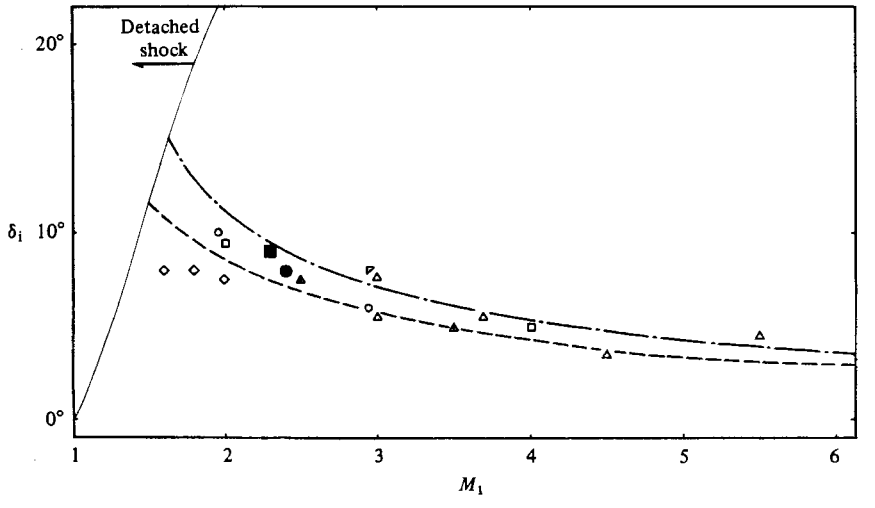

FIGURE 4. Shock-generator angle to induce incipient separation, defined according to McCabe's criterion. ■, present test; ◇, Stanbrook (1960); ○, McCabe (1966); □, Peake (1976); ◸, Oskam *et al.* (1975); △, Korkegi (1975); ▽, Neumann & Token (1974); ●, pre-exp. Kubota (1980). - — -, McCabe's theory ≃ Korkegi's criterion I, $M_1\delta_i \simeq 21°$; – – –, Korkegi's criterion II, $M_1\delta_i \simeq 17°$.

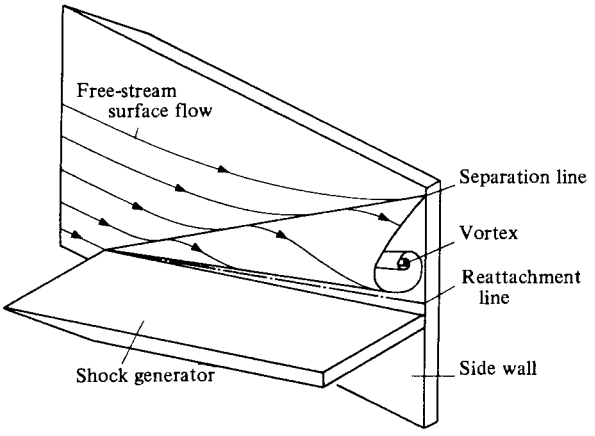

FIGURE 5. A vortex-dominated flow-field model, as suggested by Token (1974).

oil-flow pictures, vapour and smoke-screen photographs, wall-pressure distributions and local heat transfer. Our results, like Oskam's, show that separation on the side wall does not always appear when the surface-flow deflection angle exceeds the inviscid-shock angle and hence McCabe's criterion for incipient separation is conservative. Our measurements can be interpreted by the double-viscous-layer flow-field model outlined later.

2. Experiments

The experiments were made in the College of Aeronautics 23×23 cm continuous supersonic tunnel at a test Mach number of $2{\cdot}30 \pm 0{\cdot}05$. The reservoir pressure was preset at $0{\cdot}27 \pm 0{\cdot}01$ bar. The test boundary layer growing on the side wall of the tunnel was fully turbulent with a 99·5% thickness δ of 1·6 cm. The corresponding displacement and momentum thicknesses were $\delta^* = 0{\cdot}38$ cm and $\theta = 0{\cdot}1$ cm respectively. The Reynolds number per cm in the test section was $3{\cdot}1 \times 10^4$.

The model geometry was similar to that shown in figure 1. The shock generator had a chord of 15 cm, and a span of only 18 cm, to avoid reaching the opposite wall. The shock generator angle δ_s could be varied between 0 and 15°. The leading edge always remained clear of the boundary layer on the bottom liner of the tunnel. The two co-ordinate systems used in presenting the data are shown in figure 1 (*b*).

Oil-flow pictures

A mixture of titanium dioxide suspended in motor oil was used with a little oleic acid to avoid coagulation. Test surfaces were painted matt black to provide the greatest photographic contrast. Pictures of the oil patterns obtained on both the side wall and the shock generator are shown in figures 6 (*a–e*) whilst figure 7 sketches the salient features from the oil flow pictures. (In figure 7, two different 'convergence lines' are shown, one on the side wall, the other on the shock-generator surface. To avoid confusion between them, they are labelled *A* and *B* respectively.)

Surface-flow patterns on the tunnel side walls

Concentrating initially on the side wall, the oil-flow pictures show that even at the lowest wedge angles ($\delta_s = 7°$ and 9°, figures 6*a*, *b*) there are two important flow

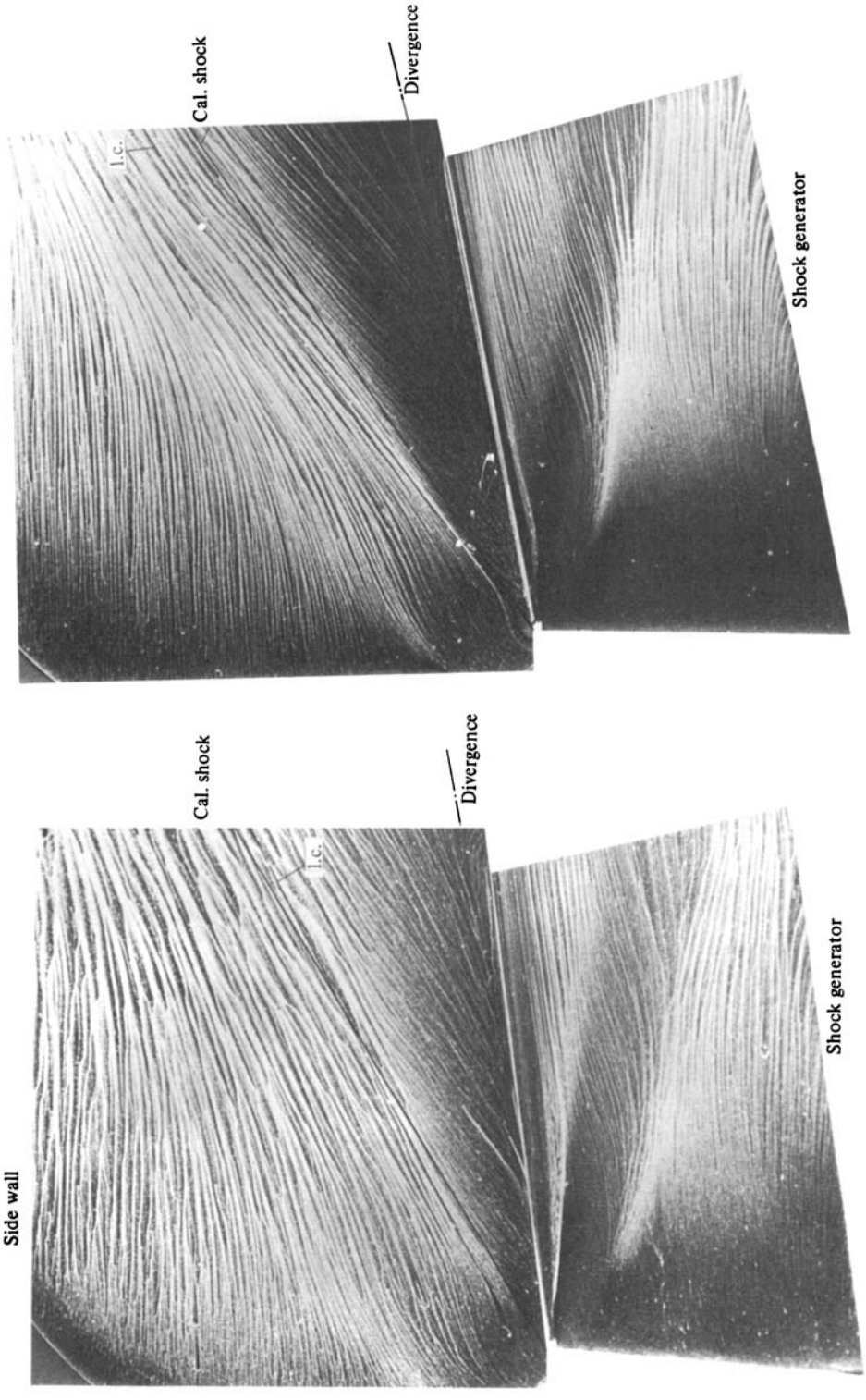

FIGURE 6 (*a*, *b*). Legend on p. 439.

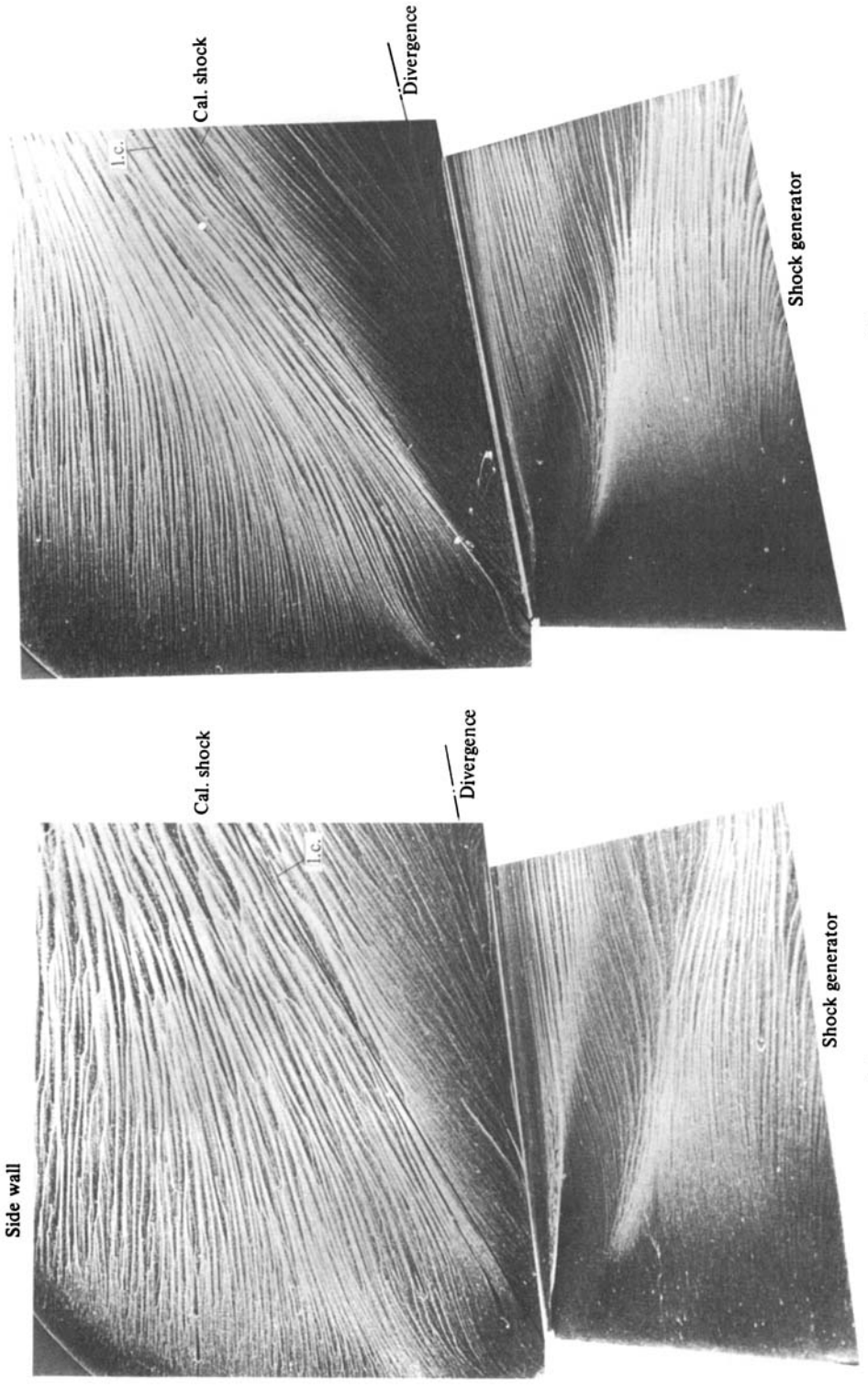

FIGURE 6 (*c*, *d*). Legend on facing page.

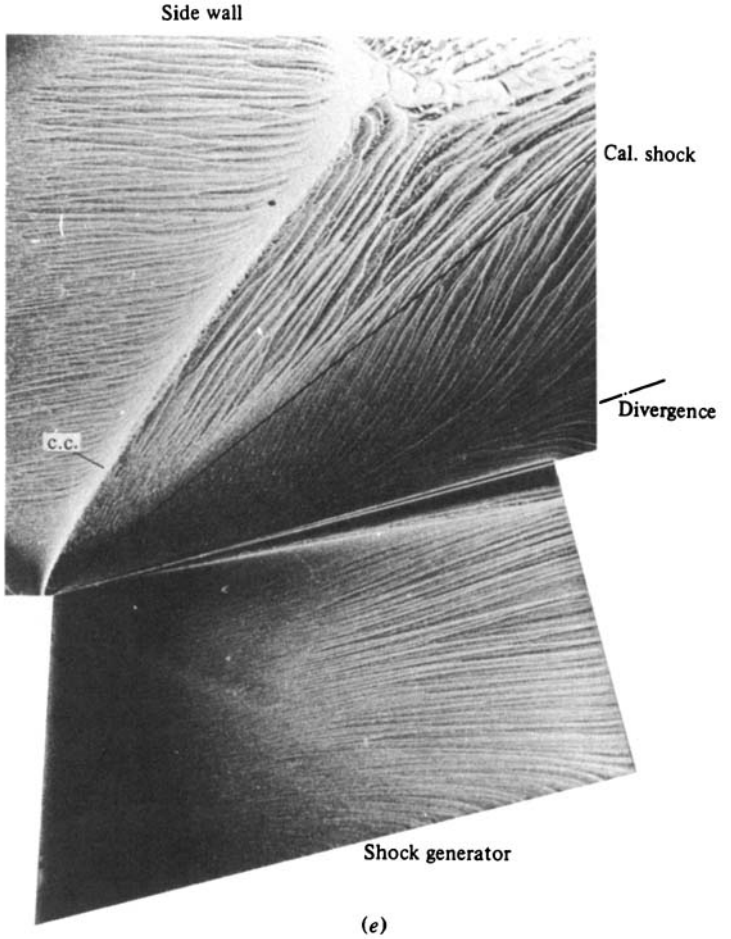

FIGURE 6. Oil-flow pictures: (*a*) $\delta_s = 7°$; (*b*) 9°; (*c*) 11°; (*d*) 13°; (*e*) 15°.

features. Well upstream of the inviscid shock the surface flow begins to turn and the surface lines start to converge, whilst near the corner there is evidence of flow divergence from a line just above the shock generator root.

(i) *Surface-flow convergence.* Following through the figure sequence (6*a–e*) it can be seen that the surface flow first turns to form what is labelled as an incomplete convergence (i.c.). For $\delta_s = 9°$ (figure 6*b*) the surface flow has already turned through an angle greater than the inviscid-shock-wave angle, but although the lines are converging there is no evidence of a single 'complete convergence'† line, which is one of the conventional indicators of separation.

However, as the wedge angle δ_s is increased, so the convergence intensifies, and at 11° a complete convergence line is evident in the lower third of the oil-flow pattern. Further increases in wedge angle enlarge the span of the complete convergence line and by 15° the whole side wall is covered, though the top of the picture is confused by boundary-layer separation on the roof of the tunnel test section. The growth of the complete convergence line is plotted against δ_s in figure 8, and compared with two sets of pilot measurements made in the much smaller 6 cm tunnel. In those tests the

† Labelled c.c. in the figures, e.g. figure 6(*d*).

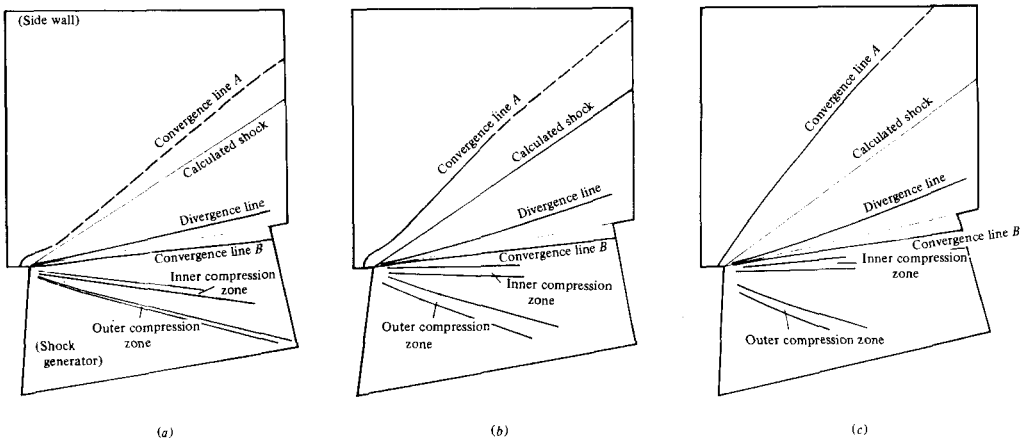

FIGURE 7. Sketches of typical oil-flow pictures: (*a*) $\delta_s = 10°$; (*b*) 11°; (*c*) 13°.

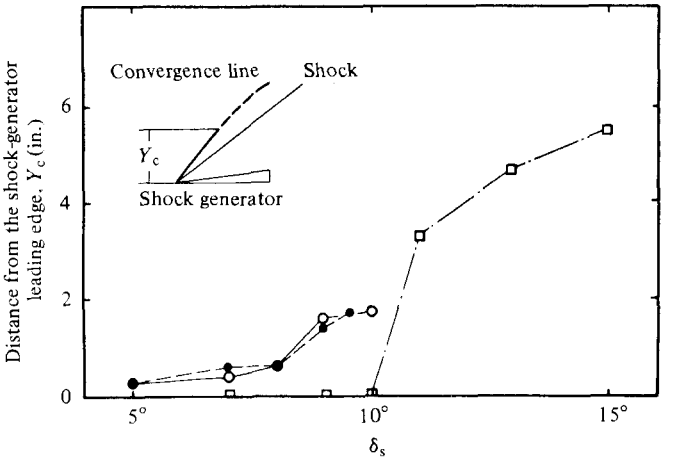

FIGURE 8. Growth of complete convergence line. ○, pre-exp. 1; ●, pre-exp. 2; □, present test.

shock generator spanned the tunnel and was mounted on the floor of the test section, so that it 'scooped up' the thick boundary layer growing along that surface. The comparison serves to emphasize the importance of local differences in test geometry.

Figures 6*c–e* show strong convergence lines lying well upstream of the inviscid shock location. Just behind (i.e. downstream of) the convergence line the oil streaks seem to lie roughly parallel to each other, instead of being drawn forwards to form the familiar herringbone pattern so often found in three-dimensional separated flows. Closer inspection shows a few streak lines entering the rear of the complete convergence, but the overall impression is one of a rather sluggish zone between the convergence line and the calculated inviscid shock position. The reason for this is given later though it is worth drawing attention to the elongated S-shape of the oil streaks above the divergence line.

(ii) *Surface flow divergence.* For all the values of δ_s tested, the oil-flow pictures show a divergence line on the side wall, close to the corner. The line seems to originate from the leading-edge station and lie along a ray from that point. The divergence line

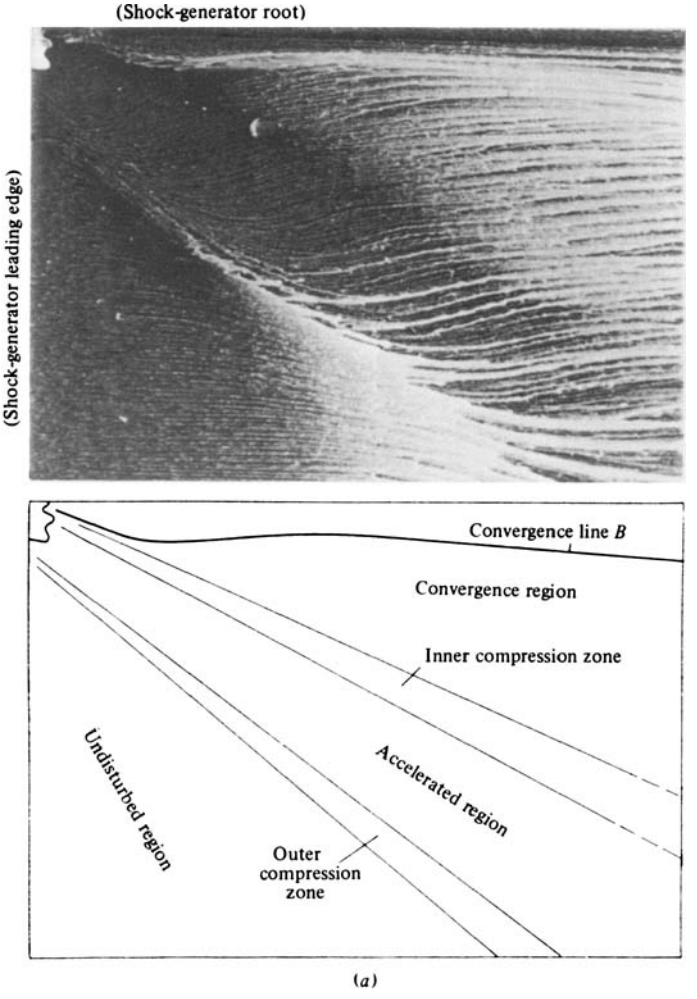

(*a*)

FIGURE 9 (*a*). Legend on p. 442

(marked 'div' in figure 6) is a characteristic of a re-attaching flow, and inspection of the shock-generator surface-flow pattern confirms this belief. Viewed from upstream, the flow travelling from left to right, there is an anticlockwise corner vortex generated by flow separating from the wedge and re-attaching to the side wall.

Surface-flow patterns on the shock generator

The lower parts of figures 6 and 7 show the oil-flow patterns on the shock-generator surface. Far from indicating a uniform flow behind an attached oblique shock wave, the pattern is quite complex, particularly at the lower wedge angles. More detailed pictures of the wedge surface flow are shown in figure 9. The angles of 10° and 13° have been chosen since they are representative of attached and separated flow conditions on the side wall.

The complexity of the patterns is due to two effects, (i) shock detachment from the leading edge of the wedge and (ii) variations of displacement thickness along the side wall. Figure 20 shows how, near the wall, within the side-wall boundary layer, the Mach number falls, resulting in shock-wave detachment. The resulting shock envelope

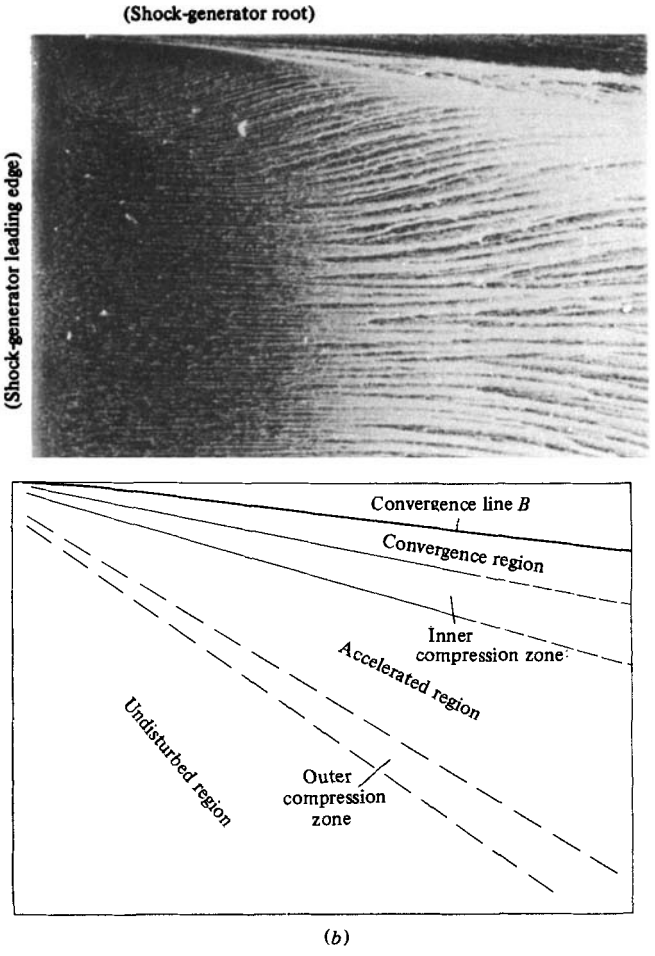

FIGURE 9. Surface-flow patterns on the shock-generator: (*a*) $\delta_s = 10°$; (*b*) 13°.

is sketched in the figure. The interaction between this envelope and the side-wall boundary layer distorts the displacement thickness and generates the undulating effective shape shown in figure 21. This in turn gives rise to a fan of compression and expansion waves which spread out over the top of the generating surface. At the larger wedge angles the sketches of the flow patterns are more indicative than the photographs (see for example $\delta_s = 13°$, figure 9*b*), since the picture had to be taken after the tunnel stopped and the oil-flow pattern deteriorated during the shut-down period.

Vapour-screen and smoke pictures

To try to understand the detailed nature of the flow field, the vapour-screen technique, as described for example by McGregor (1962), was used together with local injections of cigarette smoke to define the boundary layer.

Normally the tunnel uses dry air, but for these tests a small amount of water was injected into the settling chamber. As the air expands through the supersonic nozzle into the tunnel working section it cools, and the moisture condenses out, forming a fog. The fog particles scatter light in proportion to the number of particles per unit volume. Hence, when any cross-section of the flow is illuminated by a narrow sheet of

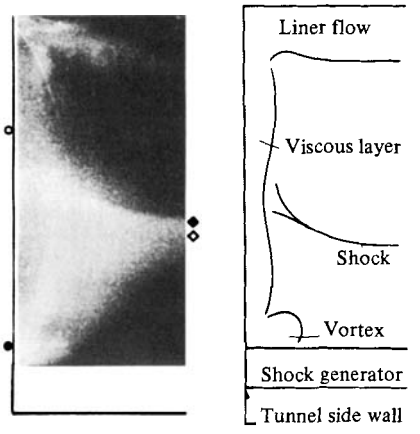

FIGURE 10. Ordinary vapour-screen picture, $\delta_s = 13°$. ○, oil-flow convergence; ●, oil-flow divergence; ◇, calculated shock position; ◆, shock position from schlieren photograph.

light, the important flow features can be seen and photographed. Figure 10 shows how the shock wave is made visible by the sudden increase in fog density. However, near the walls, where low-speed flow exists, the fog particles tend to re-evaporate and the vapour-screen picture shows a darker zone for all viscous layers. In order to distinguish one viscous layer from another smoke was injected from the points indicated in figure 11. Typical smoke and vapour-screen pictures are shown in figure 12 together with sketches depicting the way in which the photographs have been interpreted. The glancing shock, the side-wall boundary layer and the corner vortex are clearly visible in both pictures. In the upper picture (figure 12*a*) there is evidence of a viscous layer sliding over the corner vortex and infiltrating beneath the side-wall boundary layer. The corresponding oil-flow pictures suggest attached flow (apart from the corner vortex).

However, at the larger wedge angle of 13° the picture (figure 12*b*) is somewhat different. There is evidence of the shock splitting into a lambda shape near the edge of the side-wall boundary layer and a weak vortical separated region now occupies much of the layer between the corner and the shock position. The corresponding oil-flow picture suggests a separated flow as defined by the formation of a complete convergence line.

Sectional views of the corner flow are shown in figure 13, using smoke as an indicator. (The light line lying along the side wall is caused by liquid droplets produced by condensation of the smoke.) The pictures are consistent with a corner vortex located between the oil-flow convergence line B on the shock-generator surface and the oil-flow divergence line on the side wall. Smoke should accumulate in the vortex region, since this remains somewhat 'isolated' from the outer flow in which smoke particles would be rapidly dispersed. Figure 13 also suggests that the size of the corner vortex increases with distance from the shock-generator leading edge, as would be expected from the surface-oil-flow pictures.

Side-wall pressure distributions

The measurements were made using 150 pressure tappings of 0·02 in. diameter arranged in six rows parallel to the shock generator surface. The pressure distributions

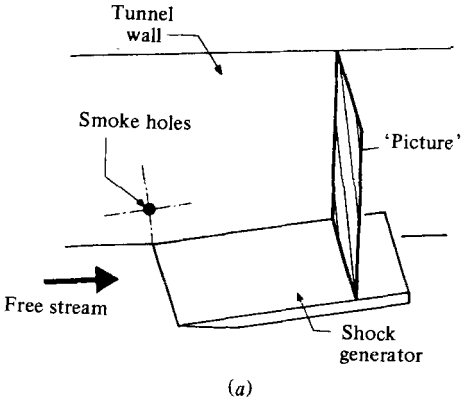

(*a*)

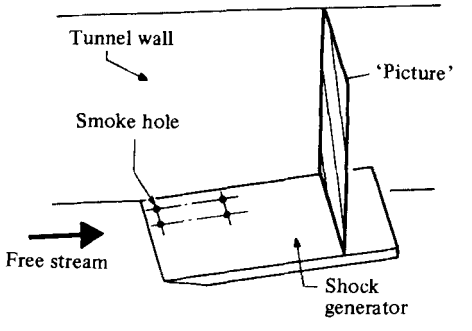

(*b*)

FIGURE 11. Smoke injections into: (*a*) side-wall boundary layer; (*b*) corner flow on shock generator.

along the rows are shown in figure 14 and from these plots the isobar patterns of figure 15 have been constructed.

Close to the corner ($Y_g = 0{\cdot}04$ in.) the pressure distribution follows the inviscid calculation reasonably well. However, with increasing distance Y_g the pressure rise becomes more gentle and occurs over a longer distance X_g. The isobar patterns (figure 15) are (very approximately) conical from an origin close to the shock-generator leading edge. This seems reasonable, since the model geometry and flow field have no characteristic length apart from the initial boundary-layer thickness δ_0.

Between wedge angles of 7° and 13° the pressure distributions develop a plateau in the region between the convergence line (the position of which is marked on figure 14) and the inviscid shock station. This plateau is particularly well shown in the distributions at $Y_g = 1{\cdot}04$ and $2{\cdot}04$ in. with $\delta_s = 13°$. The change in pressure distribution coincides with the change in oil-flow pattern from incomplete convergence at $\delta_s = 7°$ or 10° to complete convergence at $\delta_s = 13°$. The plateau pressure region is precisely that occupied by the sluggish surface oil flow behind the complete convergence line.

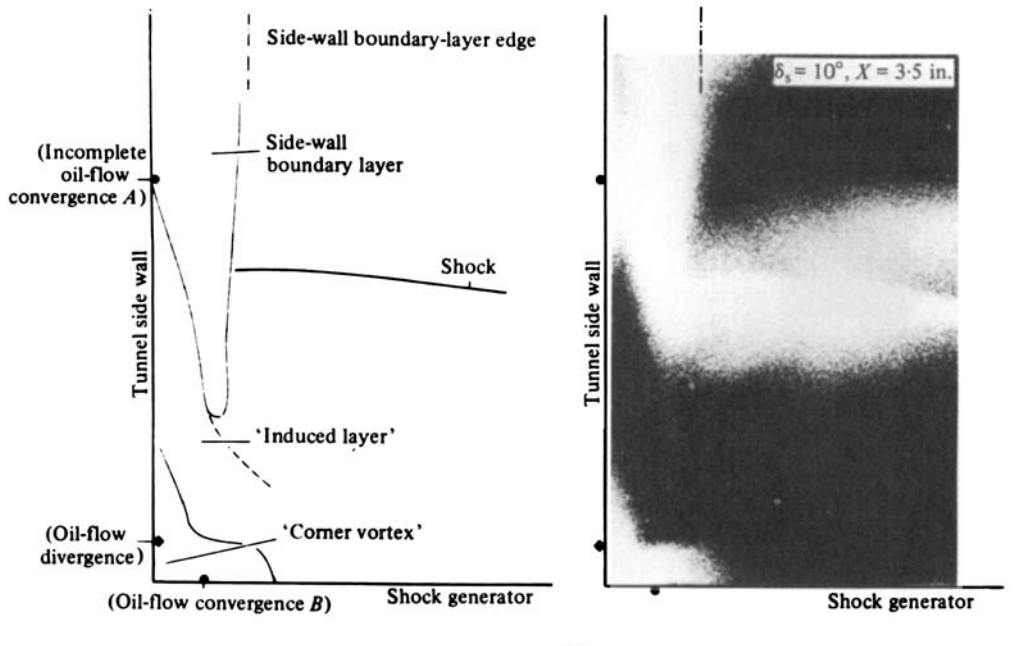

(*a*)

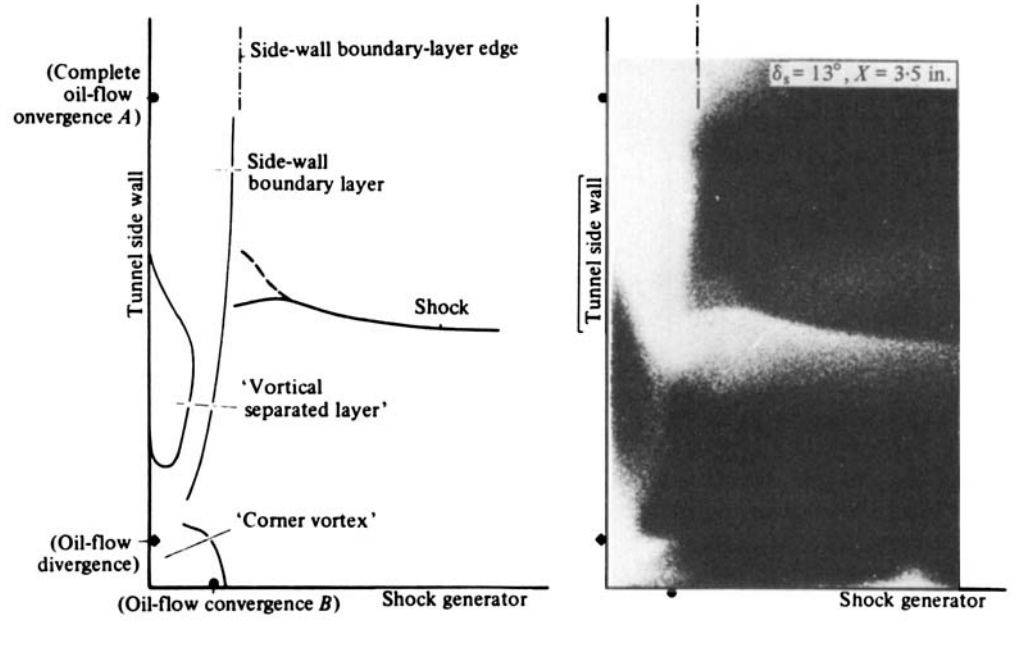

(*b*)

FIGURE 12. Vapour and smoke-screen pictures: (*a*) attached interaction region; (*b*) separated interaction region.

Heat transfer on the side wall

The heat-transfer measurements were made using a rather novel technique which is more fully described in the appendix. Basically, the method uses a 'slug' of Pyrex as a calorimeter. The calorimeter is initially heated by passing a large current through

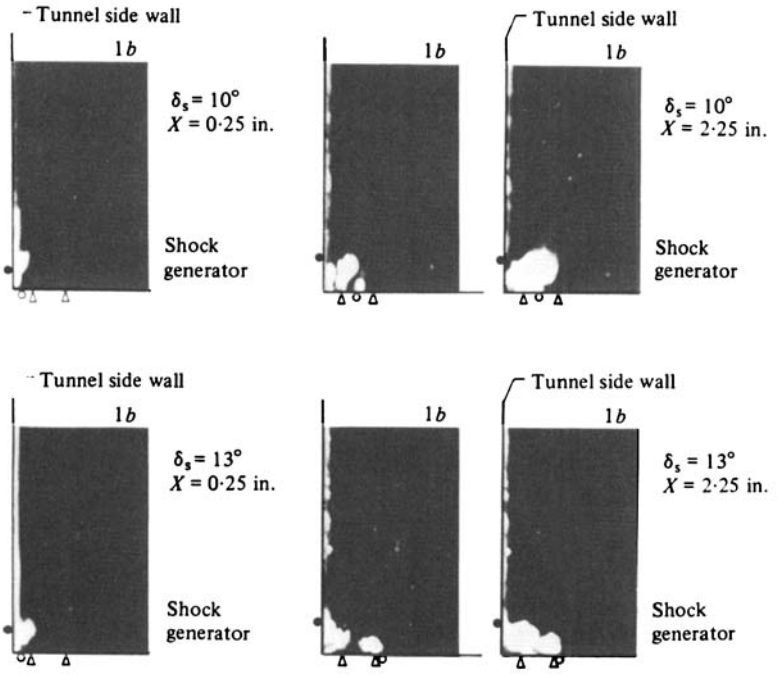

FIGURE 13. Smoke pictures at the corner region: ▽, smoke hole; ○, oil-flow convergence B; ●, oil-flow divergence; b, side-wall boundary-layer edge.

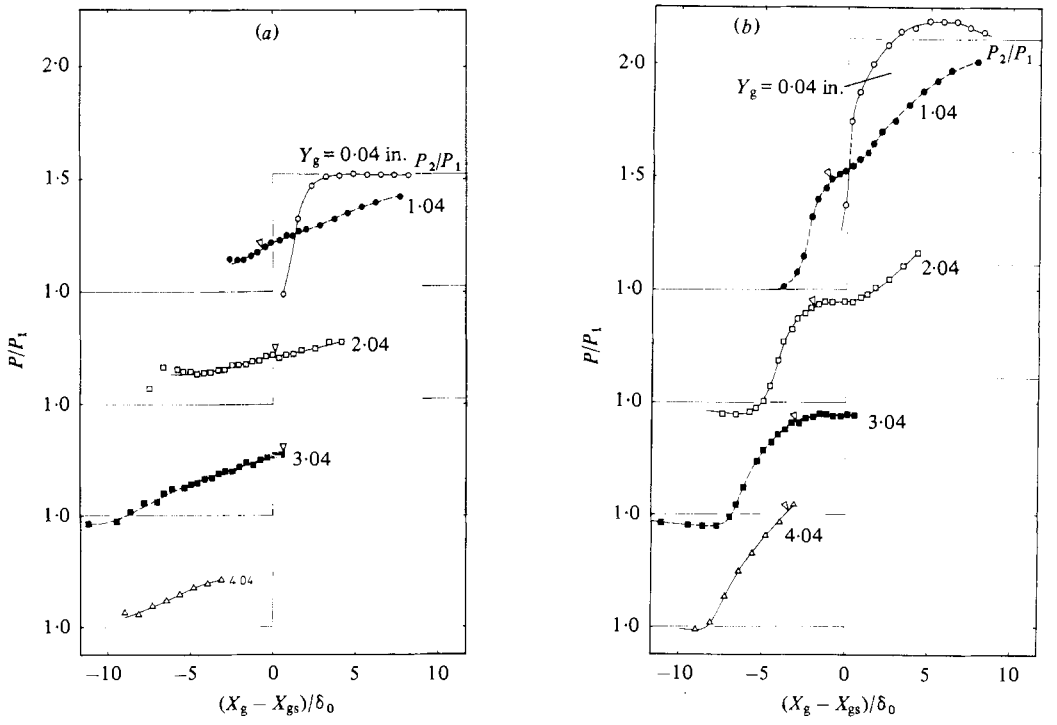

FIGURE 14. Wall-surface-pressure distributions: (*a*) δ_s = 7°; (*b*) 13°. ▽, convergence line.

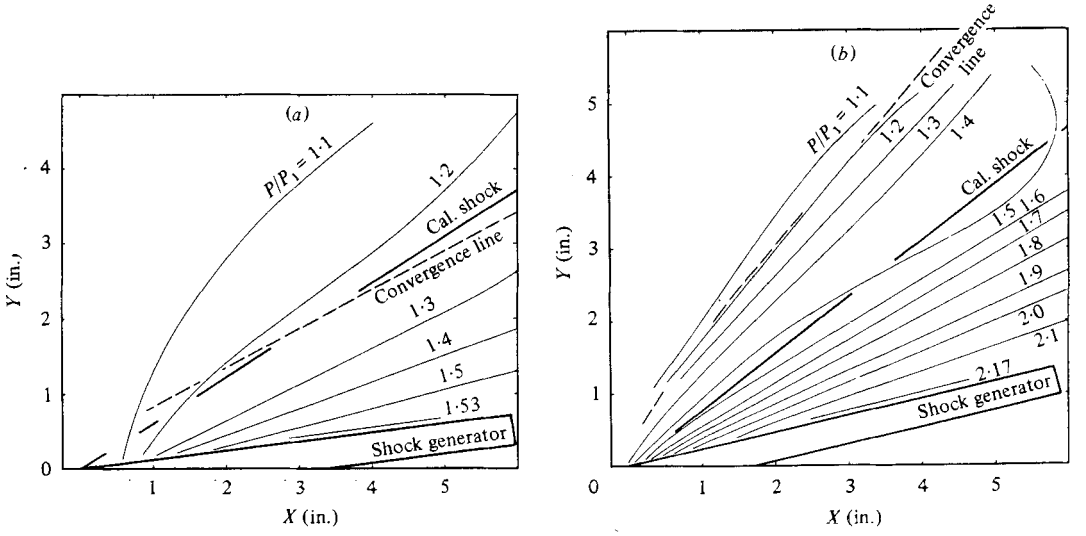

FIGURE 15. Isobar patterns on the side wall: (*a*) $\delta_s = 7°$; (*b*) 13°.

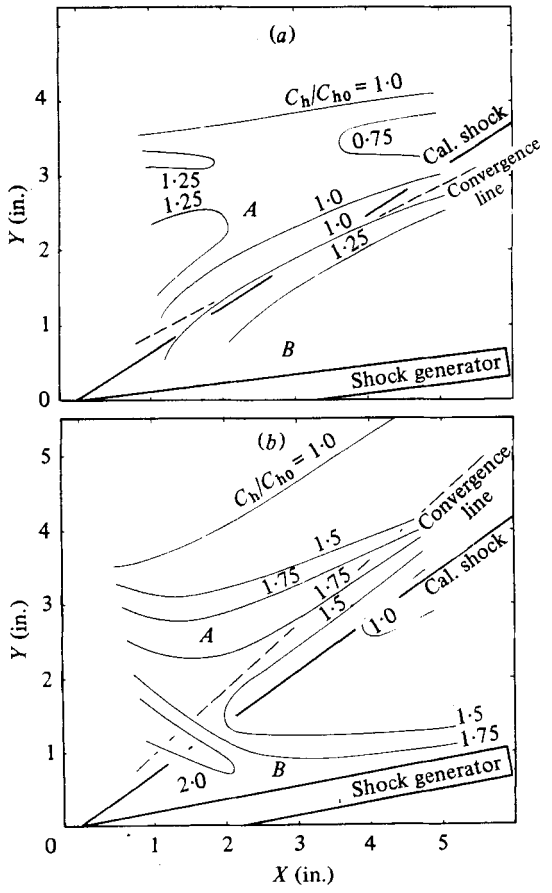

FIGURE 16 (*a*, *b*). Legend on p. 448.

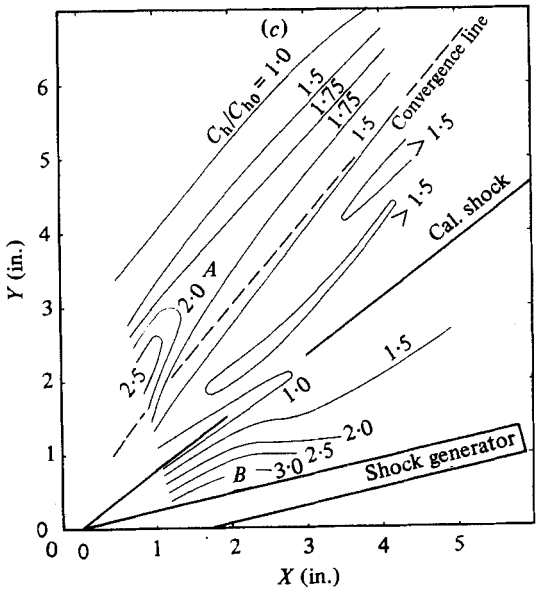

FIGURE 16. Heat transfers on the side wall: (*a*) $\delta_s = 7°$; (*b*) 10°; (*c*) 13°.

a thin-film gauge of platinum sputtered on the Pyrex. The current is then reduced and the gauge acts in a conventional way, monitoring the temperature decay of the Pyrex slug. The method was first tried without the shock generator in position. Comparisons with other flat plate boundary-layer data and theoretical estimates suggested an accuracy of $\pm 15\%$. Despite considerable care the measurements proved a little difficult to make, partly because the temperature difference between the wall and the adiabatic conditions was small (typically 18 K).

Some results are shown in figure 16 in the form of Stanton-number ratios Ch/Ch_0 with and without the shock generator present. There appear to be two regions of increased heat transfer (labelled A and B), one just ahead of the convergence line and the other in the corner of the shock generator and the side wall. Region B is associated with reattachment of the flow passing over the corner vortex while region A is connected with the high pressures and grossly distorted streamlines in the neighbourhood of the surface-flow convergence. Equally significant are the modest heat-transfer ratios in the area between the convergence line and the calculated inviscid shock, as shown in figure 16(*c*).

Of course the magnitude of the 'peak' heat transfer values are of crucial importance in design problems and many attempts have been made to correlate the experimental data. Scuderi suggested a connection between the heat transfer and pressure ratios of the form

$$\frac{Ch_{\mathrm{I}}}{Ch_0} = \left(\frac{P_{\mathrm{I}}}{P_1}\right)^{0{\cdot}85},$$

where the suffix I denotes peak values in region A, and the peak pressure P_{I} divided by the free-stream pressure P_1 is given by

$$\frac{P_{\mathrm{I}}}{P_1} = 2{\cdot}75(M_1 \sin\beta)^{\frac{1}{2}} - 1{\cdot}75.$$

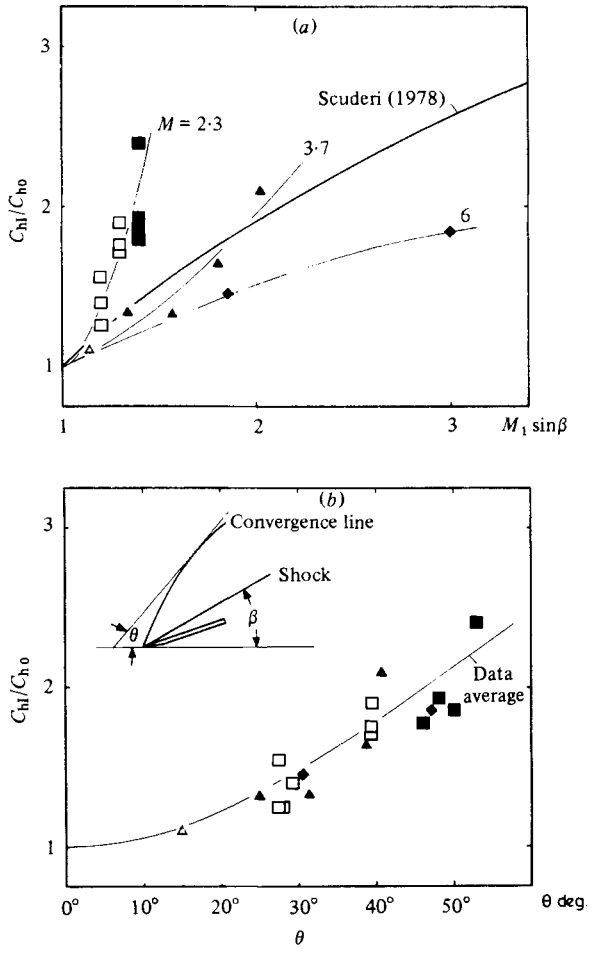

FIGURE 17. Initial heat-transfer 'peak' near the surface-flow convergence A. Correlation with (*a*) shock strength; (*b*) convergence-line angle. □, ■, present test; △, ▲, Neumann & Token (1974); ◇, ◆, Johnson & Kaufman (1978); open symbols, attached flow; filled symbols, separated flow.

Figure 17 (*a*) shows that such a prediction is unsatisfactory and figure 17 (*b*) suggests that the local angle θ of the convergence line is more relevant than the shock angle β. This is physically much more understandable, but will be no consolation to the designer until θ can be predicted.

Scuderi (1978) also attempted to predict the peak heat transfer in region B from

$$\frac{Ch_p}{Ch_0} = 1{\cdot}2\left(\frac{P_p}{P_1}\right)^{0{\cdot}85} + 0{\cdot}2,$$

where the suffix p denotes peak values in region B and the peak pressure P_p is taken as

$$\frac{P_p}{P_1} = 1{\cdot}167(M_1 \sin\beta)^{2{\cdot}2} - 0{\cdot}167.$$

Figure 18 shows these relations compared with the experimental data. The plot of heat-transfer values is notable mainly for the scatter, and we are probably deluding

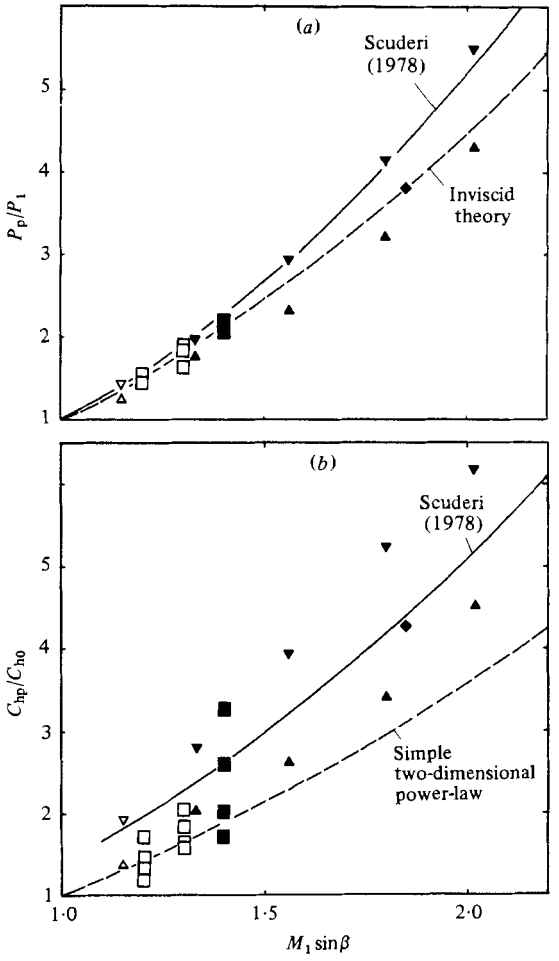

FIGURE 18. High heat-transfer 'peak' near the surface-flow divergence line: (*a*) pressure peak; (*b*) heat-transfer peak. Symbols as in figure 17, with ▽, ▼ also representing data of Neumann & Token (1974).

ourselves by believing that simple relations can be useful in a very complex flow situation which is sensitive to even minor geometric variations. A relationship for the much simpler two-dimensional shock boundary-layer interaction is also shown on the figure. It was proposed by Back & Cuffel (1970) as

$$\frac{Ch_p}{Ch_0} = \left(\frac{P_p}{P_1}\right)^{0.85}.$$

It is obvious from the comparison that three-dimensional interaction can involve more severe heat transfer than the two-dimensional case.

3. Three-dimensional separation

For ordinary separation Maskell (1955) defines a separation line as an envelope of surface streamlines converging asymptotically from both sides (figure 3*b*). Unfortunately, many of the surface-flow pictures of glancing interaction only half fulfil

Maskell's criterion. Upstream of the convergence the surface lines strongly converge and coalesce, but downstream the surface flow shows little convergence at all. However, Lighthill (1963) uses a simple mass-flow argument to clarify separation. Using a very small streamtube very close to the surface he suggests that as the surface streamlines converge and finally coalesce so the width of the streamtube must vanish and its height become infinite, i.e. the mass flux originally within the streamtube 'lifts off' and the flow separates. Hence complete convergence from the upstream side alone is enough to define separation in this way, and that is the definition used here. In our oil-flow pictures the appearance of a complete convergence line is taken to indicate separated flow.

McCabe (1966) fully supported Maskell's and Lighthill's proposals for defining three-dimensional separation. His own surface-flow pictures suggested that when complete convergence occurred the convergence line was just ahead of, but roughly parallel to, the inviscid-shock-wave position. Moreover, away from the nose region of the shock generator the flow looked approximately two-dimensional. McCabe therefore postulated a quasi-two-dimensional model of the flow and suggested that incipient separation would occur when the surface flow had turned through an angle equal to the shock-wave angle β.

Now, as our own and a number of other experiments have since shown, the surface-flow deflection angle can exceed β without a complete convergence line being formed. Moreover, the flow field can perhaps be described better as 'conical' rather than quasi-two-dimensional, though neither description is particularly apt. Thus McCabe's prediction and Korkegi's modifications to it are perhaps best interpreted as estimates of when the surface flow has turned through β, and this is what is plotted in figure 4.

As already discussed, the first appearance of a complete convergence line is a good indicator of incipient separation. However, in practice it is impossible to define the precise wedge angle for which separation starts. This is partly because of the complex flow pattern on the side wall at the nose of the shock generator and partly because the quality of the picture can be slightly affected by the properties and composition of the oil mixture. Separation starts near the root region and rapidly spreads outwards as the wedge angle is increased. Because the spread is rapid it is easier to bracket incipient separation by the attached and well-separated conditions marked on figure 19 than to pinpoint the exact value. McCabe's criterion is shown for comparison together with the theoretical shock detachment line for supersonic inviscid flow past a wedge of angle δ.

4. The structure of the flow field in the interaction region

Flow structure near the shock-generator root

The oil-flow pictures on the side wall in the region just ahead of the wedge leading edge show how the oblique shock is forced to stand off as it interacts with the boundary layer. The vapour and smoke-screen pictures clearly show the shock 'flaring out' and bifurcating as it approaches the wall in the region above and behind the wedge leading edge. Combining all this information suggests the shock envelope sketched in figure 20.

A section through this envelope taken in the plane of the wedge upper surface is shown in figure 21. The reduced Mach number in the side-wall boundary layer forces the shock to stand off, and the pressure rise across the shock propagates forward to

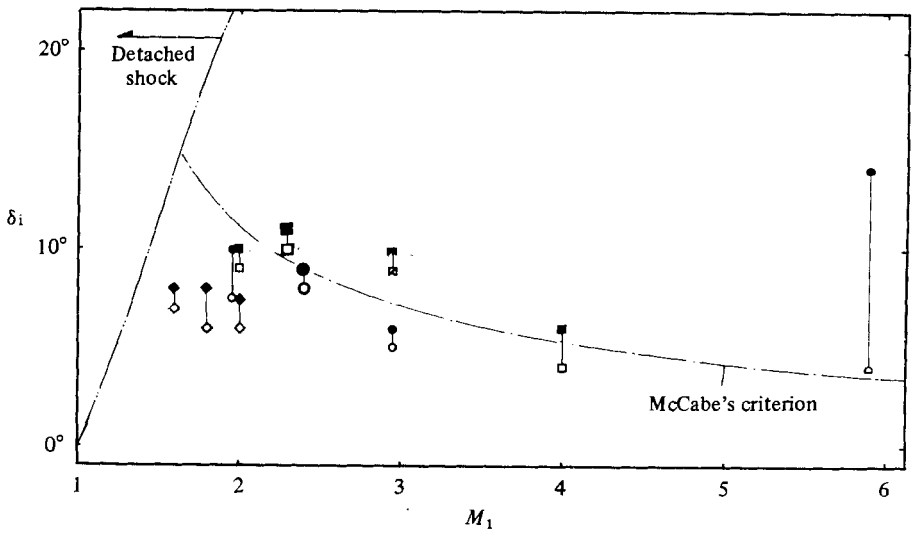

FIGURE 19. Shock-generator angle to induce incipient separation defined by complete oil-flow convergence: □, ■, present test; ○, ●, pre-exp. (Kubota 1980); ◇, ◆, Stanbrook (1960); ○, ●, McCabe (1966); □, ■, Peak (1976); △, ▲, ▽, ▼, Neuman & Token (1974); ◸, ◤, ◹, ◥, Oskam *et al.* (1975); ⌓, ◠, Goldberg (1973); open symbols, attached flow; filled symbols, separated flow.

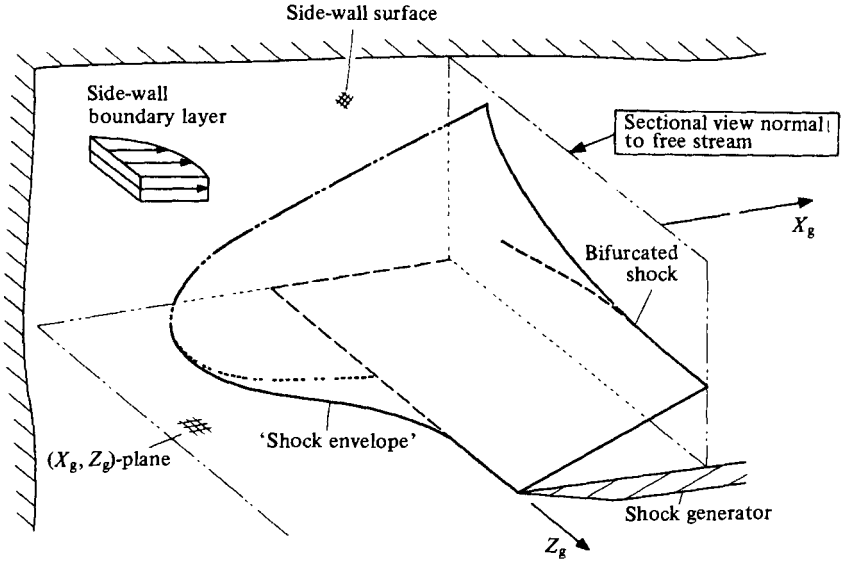

FIGURE 20. Shock envelope near the shock-generator root.

increase the local boundary-layer thickness and momentarily turn the outside stream away from the wall. Having survived the adverse pressure gradient, the boundary layer recovers and thins before returning to more normal growth along the wall. This sectional flow pattern is reminiscent of two-dimensional shock–boundary-layer interaction in which the distorted displacement thickness generates one expansion and two compressions propagating away from the surface. In our case the waves run across the wedge surface and give rise to the oil-flow patterns shown in figure 9.

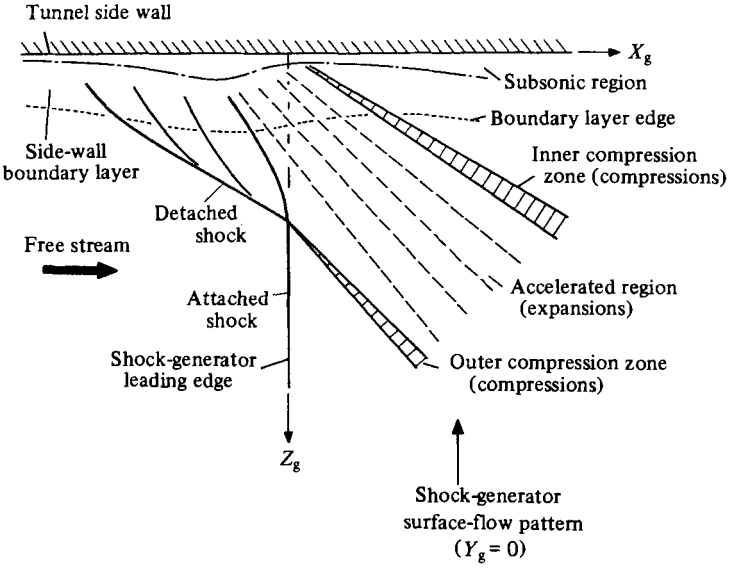

FIGURE 21. Sectional view on the (X_g, Z_g)-plane.

Flow structure on the side wall – the double-viscous-layer model

One of the most useful flow-field models was proposed by Token (1974). This model (figure 5) shows a separation vortex or bubble lying between a separation line on the side wall just ahead of the inviscid shock position and a reattachment line close to the corner and also on the side wall. This model fitted the observed convergence and divergence oil flow lines for large wedge angles and the high heat transfer measured near the reattachment line.

However, this model cannot explain all the more detailed observations that are reported here. For example, long before the appearance of a side-wall separation line there is clear evidence of an attachment line near the shock-generator root. The oil-flow pattern on the wedge shows a corresponding separation line, and the smoke pictures make it clear that there is a small corner vortex regardless of whether the rest of the side-wall flow is separated or not. There is also high heat transfer in the root region, even when the wedge angle is small. This heat transfer is clearly associated with flow reattaching above the corner vortex.

A more elaborate flow-field pattern consistent with all our observations is the double-viscous-layer model shown in figure 22. In order to understand this pattern it may help to start with the inviscid flow. The theoretical inviscid picture is easy to visualize with an attached oblique shock generating a 'slab' of high-pressure flow above the 'wing'. The slab terminates at one end in a triangular zone on the side wall. Of course the real flow has viscosity; this creates a thick side-wall boundary layer, some of which is subsonic. It is this subsonic layer that provides an 'escape route' for the high-pressure region trapped behind the inviscid shock. Basically, the high-pressure zone on the wall is relieved by forward propagation along the side surface. The pressure reduction then induces a cross flow from the wedge over onto the side wall. The cross flow meets a vertical wall and, in two-dimensional flow, would separate forming a closed bubble between the wedge and the wall. In three-dimensional flow

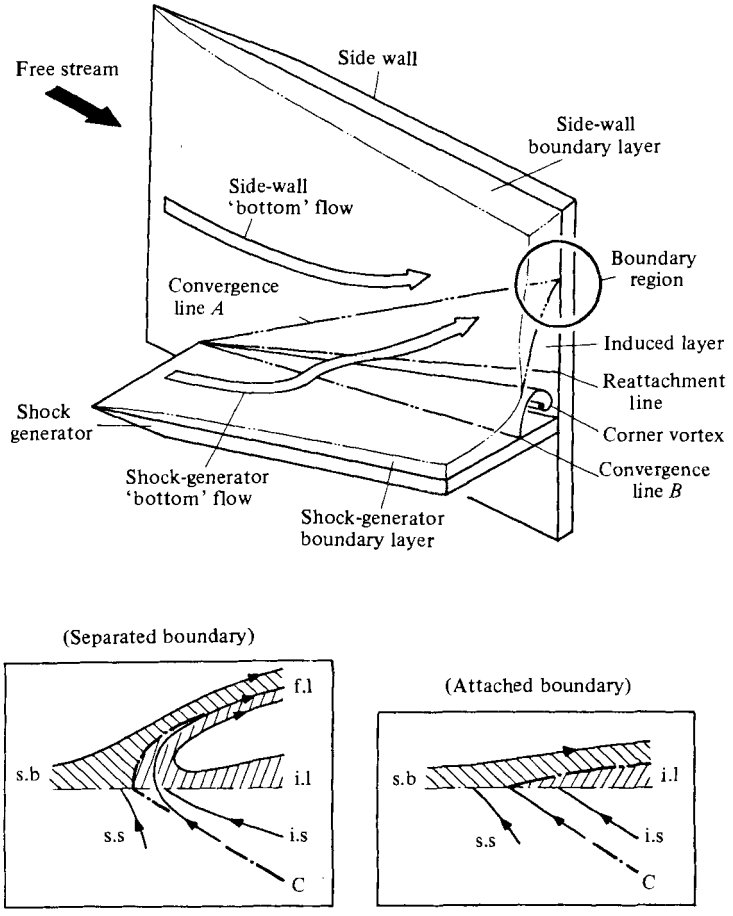

FIGURE 22. Double-viscous-layer flow-field model. C, convergence line; i.l., induced layer; i.s., induced-layer surface flow; f.l., free vortical layer; s.b., side-wall boundary layer; s.s., side-wall boundary-layer surface flow.

there is a strong axial flow component and so the flow separates to form a corner vortex. Some of the other streamtubes that are initially in the shock-generator boundary layer then flow over the corner vortex, reattach to the side wall, and infiltrate beneath the main viscous layer that has come along the wall from upstream. Thus many of the oil-flow streaklines on the lower part of the side wall are formed by flow originating close to the surface of the shock-wave generator.

Figure 22 labels the stream that slides under the main boundary layer as the 'induced layer'. As the wedge angle is increased, so the induced layer pushes further up and under the side-wall boundary layer, so deflecting the surface streamlines through a greater and greater angle (figure 23*a*). Eventually, the front edge of the induced layer presents such a large angle to the oncoming stream that the surface flow can no longer deflect around it. The wall layer then separates, lifts off from the surface, and drags the induced layer up and over, round and down, twisting to form a weak vortical flow as shown in figure 23(*b*). This vortical flow occupies nearly the whole of the interaction zone on the side wall.

Thus from our experiments it appears that the separated flow is characterized by

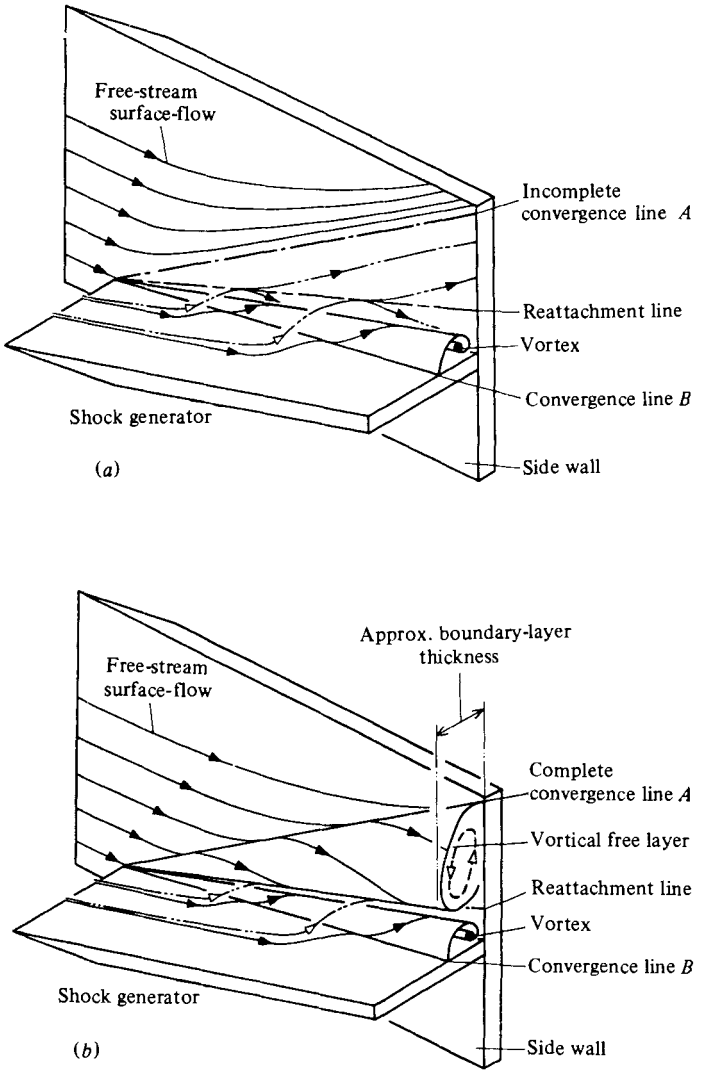

FIGURE 23. Streamlines in: (*a*) the attached flow field; (*b*) the separated flow field. —▶— , surface streamline; —▷— , free streamline.

two counter-rotating vortices, a tight, vigorous, roughly circular one in the corner with a weak, very elongated one above it. In our tests the size and shape of the vortices were such that they still did not occupy a region much thicker than the upstream boundary-layer thickness, even at the trailing-edge position of the wedge. Hence the disturbance that the viscous flow caused to the external 'inviscid' flow may have been minor. However, the vortices would be expected to grow and thus have a larger effect on the outer flow further downstream. Their main impact, as noted earlier, is to change the pressure and heat-transfer distributions in the interaction region quite dramatically.

5. Final remarks

The three-dimensional interaction region brought about by an oblique shock wave glancing across a turbulent boundary layer consists of two distinct viscous layers:

(i) the side-wall boundary layer growing along the flat surface;

(ii) the induced layer originating on the shock-generator surface near the root and crossing the path of the wide-wall layer.

Between these two viscous layers, an ordinary flow separation can occur.

Using Lighthill's argument on the behaviour of limiting streamlines near a separation line, the ordinary separation found here can be defined by the appearance of a complete surface-flow convergence, although the oil streaklines converge from the upstream side only. An additional characteristic of the separated-flow region is a plateau in the side-wall pressure distribution.

The surface-flow deflection angle on the side wall can sometimes exceed the inviscid-shock-wave angle without separation occurring. Thus McCabe's criterion for incipient separation is not always valid.

The high-heat-transfer zones are associated with the strong flow convergence ahead of the shock and with the flow reattachment line above the corner vortex. The corner reattachment produces the highest heat transfer and the importance of this region increases with Mach number.

The present study enjoyed the financial support of the United States Air Force (under grant AFOSR-76-3006 monitored by Richard Neumann) and the Japan Defense Agency. This paper represents part of the Ph.D. thesis by H. Kubota.

It is a pleasure to acknowledge the invaluable help of the Aerodynamics Department workshop staff under the able leadership of Mr S. Clark.

Appendix. Thin-film gauge calorimeter technique

The thin-film gauges were sputtered on a Pyrex glass plate in the usual way. By operating the cooler of the supersonic tunnel at maximum conditions it was possible to hold the stagnation temperature about 20 K below 'reference' wall temperature T_w. The thin-film gauge to be used was first employed as a heater by passing a steady current of about 30 mA through it. Thus a certain volume of the glass plate in the neighbourhood of the gauge was heated to around 5 K above T_w, as shown in figure 24. The current was then reduced to 3 mA and the gauge operated in the usual way as a thermometer measuring the temperature T_g of the local volume of substrate (which acts as a calorimeter). By comparing the time–temperature history, figure 25, with the corresponding record for wind-off conditions, the heat-transfer coefficient can be obtained. With reference to figure 24 the heat balance is

$$C\frac{dT_g}{dt} = h_w(T_w - T_g) - h_a(T_g - T_a), \tag{A 1}$$

where T_a is the adiabatic wall temperature.

Assuming that the heat transfer coefficients h_a and h_w are independent of tempera-

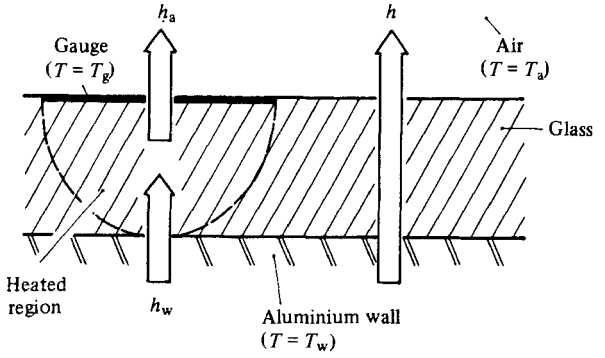

FIGURE 24. Thermal model.

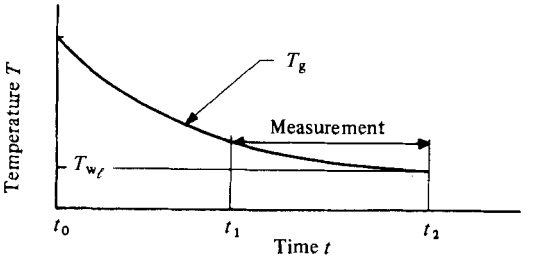

FIGURE 25. Temperature–time history.

ture and that the temperatures T_a and T_w are independent of time t, then (A 1) may be rewritten as

$$C\frac{dT_g}{dt} + (h_a + h_w)(T_g - T_a) = h_w(T_w - T_a), \tag{A 2}$$

where the right-hand side is now independent of t. The appropriate solution is

$$\frac{T_g - T_{w_\ell}}{T_{gi} - T_{w_\ell}} = \exp\left[-\frac{h_a + h_w}{C}t\right], \tag{A 3}$$

where suffixes i and ℓ denote initial and local values.

A plot of $T_g(t)$ will therefore provide $(h_a + h_w)/C$, where C is a known thermal capacity and h_w can be obtained from wind-off measurements (as heat loss). Full details are given in Kubota (1980).

REFERENCES

BACK, L. H. & CUFFEL, R. F. 1970 Changes in heat transfer from turbulent boundary layers interacting with shock waves and expansion waves. *A.I.A.A. J.* **8**, 1871–1873.

GOLDBERG, T. J. 1973 Three-dimensional separation for interaction of shock waves with turbulent boundary layers. *A.I.A.A. J.* **11**, 1573–1575.

HAYS, J. R. 1977 Prediction techniques for the characteristics of fin generated three dimensional shock wave/turbulent boundary layer interaction. *A.F.F.D.L. TR*-77-10.

JOHNSON, C. B. & KAUFMAN, L. G. 1978 Heat-transfer distributions induced by elevon deflections on swept wings and adjacent surfaces at Mach 6. *N.A.S.A. TM* 74045.

KAUFMAN, L. G. & JOHNSON, C. B. 1977 Pressure distributions induced by elevon deflections on swept wings and adjacent end-plate surfaces at Mach 6. *N.A.S.A. TM* X-3470.

KORKEGI, R. H. 1973 A simple correlation for incipient separation of a turbulent boundary layer due to a skewed shock wave. *A.I.A.A. J.* **11**, 1578–1579.

KORKEGI, R. H. 1975 Comparison of shock-induced two and three dimensional incipient turbulent separation. *A.I.A.A. J.* **13**, 534–535.

KUBOTA, H. 1980 A study of the interaction between a glancing shock wave and a turbulent boundary layer. PhD thesis, Cranfield Institute of Technology. Also: Investigations of three-dimensional shock wave boundary layer interactions. *Cranfield Institute of Technology, College of Aero. Rep.* no. 8001.

LIGHTHILL, M. J. 1963 Attachment and separation in three-dimensional flow. In *Laminar Boundary Layers*, pp. 72–82. Oxford University Press.

MCCABE, A. 1966 The three-dimensional interaction of a shock wave with a turbulent boundary layer. *Aero. Quart.* **17**, 231–252.

MCGREGOR, I. 1962 Flow visualization in wind tunnels using indicators. *AGARDOgraph* **70**, 111–164.

MASKELL, E. C. 1955 Flow separation in three dimensions. *R.A.E. Rep. Aero.* no. 2565.

MYRING, D. F. 1975 Pressure rise to separation in cylindrically symmetric shock wave–turbulent boundary layer interaction. *AGARD CP* 168.

NEUMANN, R. D. & HAYS, J. R. 1977 Prediction techniques for the characteristics of the 3-D shock wave turbulent boundary layer interactions. *A.I.A.A. J.* **15**, 1469–1473.

NEUMANN, R. D. & TOKEN, K. H. 1974 Prediction of surface phenomena induced by three-dimensional interactions on planar turbulent boundary layers. *Int. Astro. Fed. 25th Congr., Paper* no. 74-058.

OSKAM, B., BOGDONOFF, S. M. & VAS, I. E. 1975 Study of three-dimensional flow fields generated by the interaction of a skewed shock wave with a turbulent boundary layer. *A.F.F.D.L. TR*-75-21.

PEAKE, D. J. 1976 Three-dimensional swept shock/turbulent boundary layer separations with control by air injection. *N.R.C. Aero. Rep. LR*-592.

SCUDERI, L. F. 1978 Expressions for predicting 3-D shock wave/turbulent boundary layer interaction pressures and heating rates. *A.I.A.A. Paper* no. 78-162.

STANBROOK, A. 1960 An experimental study of the glancing interaction between a shock wave and a turbulent boundary layer. *A.R.C. CP* 555.

TOKEN, K. H. 1974 Heat transfer due to shock wave/turbulent boundary layer interactions on high speed weapon systems. *A.F.F.D.L. TR*-74-77.